Cluster formation in star–linear polymer mixtures: Equilibrium and dynamical properties

ARTICLE *in* SOFT MATTER · MARCH 2012

Impact Factor: 4.03 · DOI: 10.1039/C2SM06849D

3 AUTHORS, INCLUDING:

Sergei Egorov
University of Virginia
91 PUBLICATIONS **1,956** CITATIONS
SEE PROFILE

Christos N Likos
University of Vienna
216 PUBLICATIONS **6,419** CITATIONS
SEE PROFILE

Soft Matter

Cite this: DOI: 10.1039/c2sm06849d

www.rsc.org/softmatter

PAPER

Cluster formation in star-linear polymer mixtures: equilibrium and dynamical properties

Manuel Camargo,*[abc] Sergei A. Egorov[d] and Christos N. Likos[a]

Received 28th September 2011, Accepted 23rd November 2011
DOI: 10.1039/c2sm06849d

We investigate the influence of the addition of polymer chains on suspensions of low-functionality star polymers in the dilute star regime. We focus on the structural and dynamical features of the mixture by means of Molecular Dynamic simulations, based on a recently introduced model, which coarse-grained the interactions between the two components of the system. Numerical results are compared to the analytical ones, obtained from mode-coupling theory. We find evidence for the formation of transient star clusters upon chain addition, which is induced by the depletion attraction between the stars. Contrary to the case of hard colloids with a depletion-induced short-range attraction and a long range repulsion, the formed clusters are irregular and transient, allowing for particle exchange among themselves.

1 Introduction

The capability to tune the interactions between colloidal particles from short-range repulsions to long-range attractions and combinations thereof has become a valuable tool for the study of fundamental and practical problems in soft matter physics. For example, in colloidal suspensions the addition of short linear polymers induces a depletion attraction between the (hard) colloids, whose range and strength can be modulated, respectively, by changing the size and the concentration of the polymer. In such a depletion picture, variations of the control parameters, *i.e.*, the colloid volume fraction and the magnitude of the attractive interaction, yields to a non-trivial interplay between cluster formation, fluid–fluid phase separation and dynamical arrest.[1–3]

A richer scenario is achieved if the hard colloids are replaced by soft ones, inasmuch as the nature of the interactions between them can be finely tuned in many ways. Microgels, micelles, polymer-grafted nanoparticles, dendrimers and star polymers are soft colloids whose topology can be well described through a core and shell structure, and their size and softness can be easily adjusted by changing, for example, the cross-linking or the charge (microgels), the aggregation number (micelles), the grafted density (nanoparticles), the generation number or the spacer between generations (dendrimers) or the functionality, *i.e.*, the number of arms (star polymers). As a representative system of all those mentioned above, which additionally combines both polymeric and colloidal characteristics, star polymers offer the opportunity to explore structural and dynamical features of soft matter.[4] The understanding of these properties could give us some insights to design materials and supramolecular assemblies.

In particular, when dealing with binary mixtures of high functionality star polymers and smaller additives (star or linear polymers), multiple glassy states have been identified, which feature multiple re-entrant behaviors depending on the size asymmetry and the concentration of the additives.[5] Furthermore, the addition of linear polymer chains to a star gel (or glass) yields melting,[6] a depletion-like mechanism being the key to this effect. In the same line of work, a cluster formation of stars has been experimentally documented by a sudden increase of the hydrodynamic radius of the stars at the overlap concentration of the chains, from that of a single star to that corresponding to an aggregate of several stars, which is stabilized by the presence of the chains.[7,8]

In previous years, the necessary conditions leading to the formation of stable clusters in soft-matter systems have been subject of many investigations, both theoretical and experimental, employing "hard" colloidal models. The current understanding of the mechanism that drives the formation of stable, equilibrium clusters is based on the antagonistic role played by the short-range attractive well and the long-range repulsive tail characterizing the mutual, effective interaction between the basic entities forming in the system. Although extremely short-range attractions and long-range repulsions were initially employed,[9,10] it has been shown that also moderate values of the same can lead to the formation of clusters. Moreover, the interaction at short particle overlaps need not be hard; even the soft star-polymer type interactions

[a]*Faculty of Physics, University of Vienna, Boltzmanngasse 5, A-1090 Vienna, Austria. E-mail: manuel.camargo@univie.ac.at*
[b]*Wolfgang Pauli Institut, Vienna, Austria*
[c]*Dirección Nacional de Investigaciones, Universidad Antonio Nariño, Kra 3 Este 47a-15, Bogotá, Colombia*
[d]*Department of Chemistry, University of Virginia, McCormick Road, Charlottesville, Virginia, 22904, USA*

are sufficient.[7,8] The attractions can even be dropped, and still clusters will form if the repulsion is soft enough, allowing full particle overlaps and decaying sufficiently fast to zero at large separations.[11,12]

In this work, we address the formation of clusters in dilute suspensions of low-functionality star polymers, arising as a consequence of the addition of linear polymers (chains). Structural and dynamical properties of the stars were studied by means of numerical simulation of the binary mixture by employing a coarse-grained model, which makes use of the effective interaction between both components of the mixture, *i.e.*, star–star, chain–chain, and star–chain interactions. The rest of this article is organized as follows: In section 2 the employed coarse-grained model is described as well as some details concerning the numerical simulations. The central part of this work is presented in sections 3 and 4, where results are displayed. Finally, in section 5 we summarize and draw our conclusions.

2 Model and simulation

As mentioned previously, we describe the mixture by coarse-graining the mutual interactions between the two species forming the system, which are purely entropic in origin, *i.e.*, the system is athermal. We consider star polymers of functionality f and radius of gyration $R_g^{(s)}$ and homopolymer chains with radius of gyration $R_g^{(c)}$. A detailed description of the coarse-graining procedure is given in Ref. 13 and 14. Briefly, by taking the center of the stars and the middle monomer of the chains as effective coordinates, the coarse-grained pair interactions display an ultrasoft logarithmic dependence at short distances and cross over to an exponential decay at large ones. More explicitly, the effective interaction between two stars reads as[15]

$$\frac{V_{ss}(r)}{k_B T} = \Theta(f)\begin{cases} -\ln\left(\frac{r}{\sigma_s}\right) + \frac{1}{1+\frac{\sqrt{f}}{2}} & r \le \sigma_s \\ \frac{1}{1+\frac{\sqrt{f}}{2}}\left(\frac{\sigma_s}{r}\right)\exp\left[-\frac{\sqrt{f}}{2\sigma_s}(r-\sigma_s)\right] & r > \sigma_s \end{cases} \quad (1)$$

where, $\Theta(f) = (5/18)f^{3/2}$, $\sigma_s \cong (4/3)R_g^{(s)}$ is a measure of its extension, k_B is the Boltzmann constant and T is the absolute temperature. Similarly, polymer chains can be considered as two-arm stars interacting *via*[16,17]

$$\frac{V_{cc}(r)}{k_B T} = \Theta(2)\begin{cases} -\ln\left(\frac{r}{\sigma_c}\right) + \frac{1}{2\mu^2\sigma_c^2} & r \le \sigma_c \\ \frac{1}{2\mu^2\sigma_c^2}\exp\left[-\mu^2\left(r^2-\sigma_c^2\right)\right] & r > \sigma_c \end{cases} \quad (2)$$

with $\mu\sigma_c = 1.03$, which guarantees the correct value of the second virial coefficient of a polymer solution. As before, $\sigma_c \cong (4/3)R_g^{(c)}$ measures the size of the chain. The cross interaction between stars and chains results[14]

$$\frac{V_{sc}(r)}{k_B T} = \begin{cases} -\hat{\Theta}(f)\ln\left(\frac{r}{\sigma_{sc}}\right) + K & r \le \sigma_{sc} \\ v_0 \int \varphi_s(r')\varphi_c(|\mathbf{r}-\mathbf{r}'|)\,d\,\mathbf{r}' & r > \sigma_{sc} \end{cases} \quad (3)$$

where $\hat{\Theta}(f) = \frac{5}{36}\frac{1}{\sqrt{2}-1}[(f+2)^{3/2} - (f^{3/2}+2^{3/2})]$, $\sigma_{sc} = (\sigma_s + \sigma_c)/2$ and v_0 is the excluded volume parameter. The latter comes from Flory-type arguments for the overlapping monomer density profiles $\varphi_\alpha(r)$ (α = s, c), which can be evaluated on the basis of the Daoud–Cotton blob model and are given by[14,18]

$$\frac{\varphi_\alpha(r)}{A_\alpha} = \begin{cases} \left(\frac{\sigma_\alpha}{2}\right)^{-5/3} r^{-4/3} & r \le \frac{\sigma_\alpha}{2} \\ \left(\frac{1}{r^2} + 2\kappa_\alpha^2\right)\frac{2\zeta_\alpha}{\sigma_\alpha}\exp\left\{\kappa_\alpha^2\left[\left(\frac{\sigma_\alpha}{2}\right)^2 - r^2\right]\right\} & r > \frac{\sigma_\alpha}{2} \end{cases} \quad (4)$$

where A_α is a normalization constant and $\zeta_\alpha^{-1} = 1 + \kappa_\alpha^2\sigma_\alpha^2/2$. The parameter κ_α is set by $\kappa_\alpha\sigma_\alpha = 1.27$ in order to fit the theoretical profile, eqn (4), to the MD simulation results. Finally, the constants K and v_0 are determined by requiring continuity of both $V_{sc}(r)$ and its first derivative at $r = \sigma_{sc}$.

The validity of the coarse-grained interaction potentials, *i.e.*, eqn (1)–(3), has been demonstrated by computer simulations[14] as well as by robust experimental evidence describing the features of mixtures of star-like micelles and homopolymer chains. Quantitative, parameter-free agreement between experiment and theory for the pair correlations and the phase behavior was achieved in a wide range of polymer concentrations, beyond the overlapping one.[19,20]

In order to study the static and dynamic features of the coarse-grained mixture of star- and linear polymer, we performed Molecular Dynamics simulations for several combinations of densities $\rho_\alpha = N_\alpha/V$ (α = s, c), N_α being the number of particles of the species α and V the total volume. The range of star density was kept well below its overlap value ρ_s^*, *i.e.*, $\rho_s < 0.4\rho_s^*$, with $\rho_s^*\sigma_s^3 \cong 0.57$. Mixtures of star- and linear polymer characterized by a fixed chain-to-star size ratio $\xi = \sigma_c/\sigma_s = 0.5$ and functionalities f = 12, 18, 24 were used as representative systems. Newtonian equations of motion were integrated by means of the velocity Verlet scheme,[21] with a time step $\Delta t/\tau$ ranging from 0.001 to 0.005, where $\tau = \sqrt{m_s\sigma_s^2/k_B T}$. The chain-to-star mass ratio was chosen as $m_c/m_s = 0.2$. The size of the (cubic) simulation box, L_{box}, was typically 14 to 20 times the star diameter σ_s and periodic boundary conditions were considered.

Initial configurations were generated by randomly placing the particles in the box. By setting the scale of energy as $k_B T = 1$, an equilibration run was performed in which the system was thermalized by periodic velocity rescaling. The typical equilibration time ranged from 5×10^5 to 10^6 time steps according to the studied chain density. After reaching equilibrium, indicated by the absence of any drift in internal energy and pressure, a production run was performed in the microcanonical ensemble, at different densities and compositions. Typical production runs ranged from 8×10^5 to 2×10^6 time steps.

We compared simulation results for the star diffusion coefficient and density correlation functions with those computed on the basis of the mode-coupling theory, which requires structural information as input. The latter was obtained from a thermodynamically self-consistent integral equation theory, namely, information about both center-to-center radial correlation functions $g_{\alpha\beta}(r)$ and structure factors $S_{\alpha\beta}(q)$ ($\alpha, \beta \in$ {s, c}) gained by solving the two-component Ornstein–Zernike equations within the hypernetted-chain (OZ-HNC) approximation.[22]

3 Static cluster properties

The structural information can be obtained by means of the partial structure factors $S_{\alpha\beta}(q)$, which are related to the propensity of a fluid to sustain spontaneous density fluctuations of wave vector q. They are evaluated as

$$S_{\alpha\beta}(q) = \frac{\langle \rho_\alpha(q,0)\rho_\beta(-q,0)\rangle}{\sqrt{N_\alpha N_\beta}} \quad (5)$$

with $\rho_\alpha(q,t) = \sum_{j=1}^{N_\alpha} \exp[i\,\mathbf{q}\cdot\mathbf{r}_{\alpha,j}(t)]$, the sum is performed over the coordinates $\mathbf{r}_{\alpha,j}$ of particles of type α, and $\langle\rangle$ denotes a statistical average. Fig. 1 displays the star–star structure factor $S_{ss}(q)$ for $f = 18$ and different chain densities. As ρ_c increases, the nearest-neighbor peak of $S_{ss}(q)$ (located at $q_n\sigma_s \sim 4$) shifts to larger q, pointing out that the distance between (star–star) nearest-neighbors decreases. In contrast to colloid/polymer mixtures, where the shift is nearly independent of the polymer density,[3] in the present case, it grows monotonically as a consequence of the softness of the stars, which allow them to overlap when they are pushed together. Concomitantly, the height of the peak decreases at first and then increases again, suggesting an increase of the average number of nearest-neighbors. That this is indeed the case is demonstrated in Fig. 2, which displays the distribution of the number of (star–star) nearest-neighbors (N_{nn}) extracted from MD simulation snapshots. We consider two stars as neighbors if the distance between their centers is smaller than $R_{cutoff} = 1.5\sigma_s \cong 2R_g^{(s)}$, with $R_g^{(s)}$ the radius of gyration of the star, *i.e.*, when the outer part of the star shells begin to overlap. As can be seen in Fig. 2, as the chain density is increased, the occurrence of isolated stars becomes less probable and at the higher chain density the most probable case is to find groups of three or four stars.

On the other hand, the shifting of the peak at q_n is associated to the emergence of a pre-peak at smaller q_c ($q_c\sigma_s \sim 1$), which is related to the formation of structural heterogeneities of characteristic size $l \sim q_c^{-1}$ and involving a number M_s of stars. According to previous works involving the study of interaction potentials featuring short-range attraction and long-range repulsion, such a pre-peak of the structure factor can be associated to different types of structures, depending on the combination of parameters employed to define the potential. In this way, the pre-peak of $S_{ss}(q)$ can be interpreted as defining the typical separation between well defined, stable (permanent) clusters,[9] or as defining the average size of intermediate range order structures,[23] as for example, network-like structures, which can be eventually distinguished by its (transient or arrested) dynamics.

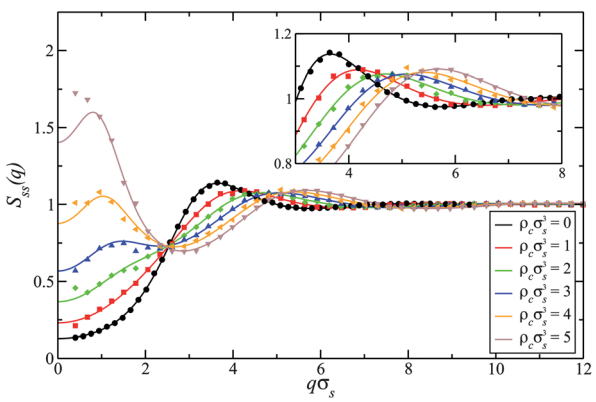

Fig. 1 Star–star structure factors as obtained from the solution of the OZ-HNC (lines) and simulation (circles) for $f = 18$, $\rho_s\sigma_s^3 = 0.1$ and different chain densities, as indicated in the legend. Inset: Zoom of the main plot around the region of the particle peak of $S_{ss}(q)$. As in all figures, results are shown for a chain-to-star size ratio $\xi = 0.5$.

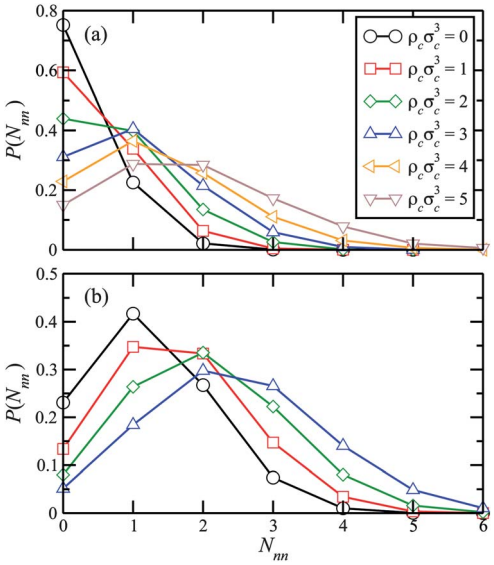

Fig. 2 The probability distribution of the number of (star) nearest-neighbors for (a) $\rho_s\sigma_s^3 = 0.1$ and (b) $\rho_s\sigma_s^3 = 0.2$ as the number of chain increases for $f = 18$.

As a first step to characterize the structures giving rise to the pre-peak in $S_{ss}(q)$, we follow Ref. 24 and estimate M_s, the number of connected stars. By definition, two stars are connected if they are themselves nearest-neighbors and simultaneously nearest-neighbors of a third star. In addition, we measured the size of each resulting aggregate by determining its radius of gyration, *i.e.*, $R(M_s) = \langle[M_s^{-1}\sum_{k=1}^{M_s}(\mathbf{r}_{s,k} - \mathbf{R}_{com})^2]^{1/2}\rangle$, where the sum is carried out on the positions $\mathbf{r}_{s,k}$ of the connected stars, $\mathbf{R}_{com}$ is the position of the corresponding center of mass and the average is carried out on all aggregates with the same M_s, which were found in many independent, instantaneous configurations of the system.

Fig. 3 displays the distribution of M_s and the average radii of gyration for $\rho_s\sigma_s^3 = 0.1$ and two different functionalities as chains are added. As can be seen, at a low chain density the stars are mainly isolated or connected at most with one other star (see also Fig. 2). By further increasing the chain density, the distribution of M_s broadens, suggesting the formation of very polydispersed aggregates, as confirmed by measuring its radius of gyration. At larger ρ_c, the distribution of the connected stars begins to display a power-law decay, coinciding this change of behavior with the rising up of the pre-peak in $S_{ss}(q)$. On the other hand, we found $R(M_s) \sim M_s^{0.5}$, which is reminiscent of the dependence occurring in structures resulting from a reaction-limited colloid aggregation (RLCA), for which $R(M_s) \sim M_s^{0.48}$ was found.[25]

It is important to note that the value of $S_{ss}(q \to 0)$ increases as the chain density does (see Fig. 1), demonstrating that the system is approaching the spinodal line and, therefore, a fluid–fluid phase separation will take place at a high enough chain density.

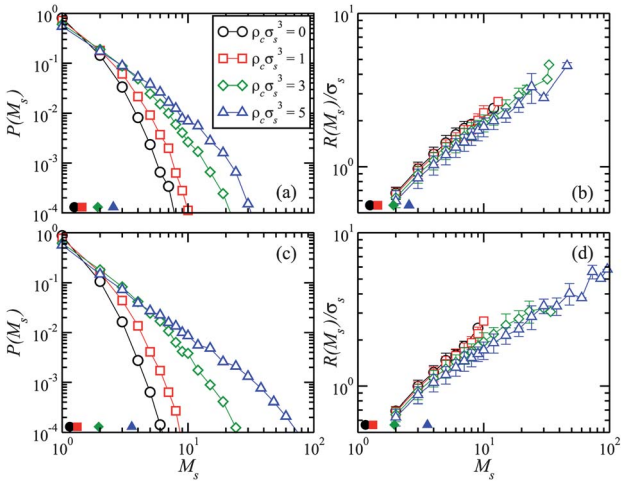

Fig. 3 Distribution of the number of connected stars $P(M_s)$ and average radius of gyration $R(M_s)$ of the corresponding aggregates for $f = 12$ [(a),(b)] and $f = 18$ [(c),(d)] as linear chains are added to the system. The star density is fixed at $\rho_s\sigma_s^3 = 0.1$. Filled symbols close to the horizontal axis indicate the average M_s.

As the star density ρ_s increases, the small aggregates (or transient clusters, as will be explained below) become larger and, as more chains are added, they can connect and span the whole simulation box. In Fig. 4 some representative snapshots of the simulation box for $f = 18$ and $\rho_s\sigma_s^3 = 0.2$ are presented, showing the number of connected particles as a fraction of the total number of stars in the simulation box. As can be seen, clusters of connected stars coarsen as the chain density increases and form a transient percolating network, in a similar way as the one found in colloid–polymer mixtures.[3,24,26]

The formation of growing star clusters upon chain addition, as well as the final demixing transition, can be explained in the framework of the depletion interaction between the stars, which is induced by the presence of smaller chains. Under this view, the mixture is adequately considered as an effective one-component star polymer solution, in which the stars do not interact through $V_{ss}(r)$ given by eqn (1), but through a chain-modified effective potential $V_{ss}^{eff}(r)$, where the degrees of freedom of the chains have been traced out (*i.e.*, a second coarse-graining procedure is performed). By construction, this chain-modified interaction leaves the correlation functions $g_{ss}(r)$ and $S_{ss}(q)$ between the stars invariant.[27,28]

As Fig. 5 displays, the addition of chains results in the reduction of the star–star repulsive potential, which can be also interpreted as a reduction of its range. This is manifested in experiments by the shrinkage of the star size due to its deformability and to the osmotic forces exerted by the chains.[29,30] By further increasing the chain density, *i.e.*, close/above its overlap concentration ($\rho_c^*\sigma_s^3 \cong 4.5$ under the conditions considered here), $V_{ss}^{eff}(r)$ features a well-and-shoulder structure, *i.e.*, it shows an attractive well at short distances and a repulsive tail at larger ones. In this way, the attractive well favors the aggregation of particles, but the size of such aggregates is thereafter limited by the repulsive tail, inhibiting the growth of an infinite cluster. The described structure of the effective potential appears to be well supported for a larger range of chain densities provided that the mixture is characterized by an intermediate size ratio ($\xi \sim 0.5$) and a low functionality ($f \lesssim 24$). On the opposite case, *i.e.*, large functionality and low size ratio, a repulsive tail is not present in $V_{ss}^{eff}(r)$ and the structure factors $S_{\alpha\beta}(q)$ diverge at $q = 0$, indicating that the system is approaching the demixing spinodal, without displaying the cluster peak.[27,28]

The aforementioned mechanism has been established to be behind the formation of stable clusters in double Yukawa fluids, as well as in lysozyme solutions at low and intermediate volume fractions.[9,10,31–34] Suspensions of particles interacting by a combination of attractive and repulsive Yukawa potentials feature cluster formation or macrophase separation, depending on the relative strength and ranges of the attractive and repulsive parts. In the first case, it is also possible to have situations in which a binodal line is preceded by a region of stability of finite clusters, *i.e.* clusters are precursors of the phase separation.[31] Concerning the structural properties of the clusters, particles featuring an effective potential consisting of a superposition of a generalized $n - 2n$ Lennard-Jones potential and a long-range Yukawa repulsion, can build up compact spherical clusters at a low volume fraction, which turn out to have a preferential size and which become more elongated at larger densities depending on the parameters defining the potential.[9,10] The latter ones were chosen in such a way that the potentials are characterized by a quite narrow attractive well ($\lesssim 5\%$ of the hard-core diameter)

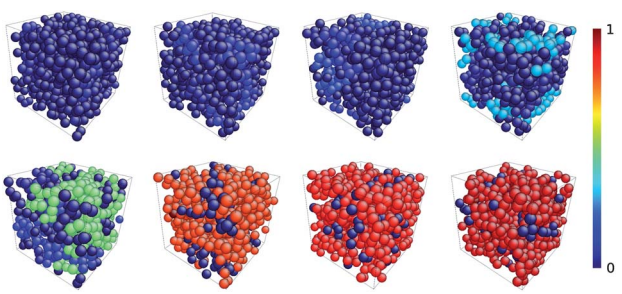

Fig. 4 Representative snapshots of the system for $f = 18$ and $\rho_s\sigma_s^3 = 0.2$ and different chain densities. From left to right and top to bottom, $\rho_c\sigma_s^3$ was increased from 0 to 3.5 in steps of 0.5. The color bar measures the fraction of connected stars in relation to their total number in the simulation box. For the sake of clarity, only stars are represented, rendered here as spheres of diameter σ_s.

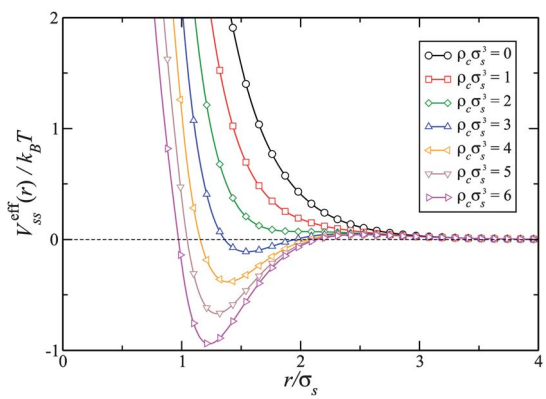

Fig. 5 Chain-mediated effective star–star potential as obtained by inversion of the OZ equation in the limit $\rho_s\sigma_s^3 \to 0$ (see Ref. 27). The influence of increasing the chain density is shown for $f = 18$ and $\xi = 0.5$.

and a moderate depth ($\gtrsim 2k_BT$). These characteristics of the potential render in a very sharp pre-peak of the structure factor, setting a well defined distance between clusters. On the contrary, in the system under investigation, the attractive part of the effective potential $V_{ss}^{eff}(r)$ is relatively shallow ($\lesssim k_BT$) and wide ($\sim\sigma_s/2$), leading to much more diffuse and transient clusters.

Aggregates with compact structures have been also reported for colloid/polymer mixtures, in which the cluster morphology does not depend on the colloid volume fraction but on the range of the depletion interaction, which can be tuned by changing the polymer size.[2,24] In that case, "long" polymers ($\xi \sim 0.15$) allow the formation of compact clusters, while for shorter polymers ($\xi \sim 0.02$) the clusters become branched. Note that in the colloid/polymer mixtures, the effective potential between the colloids does not exhibit the long range repulsion, which appears to be the key in the former model to the inter-cluster stabilization at low volume fractions.[9,10]

Due to the rather low repulsive barrier of $V_{ss}^{eff}(r)$ for the system under study (see Fig. 5), it would be reasonable to employ the same arguments as for the colloid/polymer mixtures and to argue that the above described mechanics for the cluster formation in star/linear polymer mixtures could be easily modulated by changes in the size ratio ξ, as described previously. However, the two systems bear an important difference. Whereas the depletants of hard spheres set up both the range and the strength of the depletion potential, in the case of (soft) core–shell spheres is the depleted particle which plays the major role in determining it. As consequence of the penetrability of the shell, it has been demonstrated that the range of the corresponding depletion potential has a very weak dependence, not only on the chain density but also on the size ratio (at least in the range $0.1 \leq \xi \leq 0.5$).[28]

Summarizing, for the mixture under study, the aggregation of stars in small clusters is set by the development of a minimum in the effective potential $V_{ss}^{eff}(r)$ as the chain density increases; however, these clusters are not sufficiently stabilized by the weak repulsive Yukawa tail of $V_{ss}(r)$, being this effect more evident at larger functionalities and/or smaller size ratios. Due to the shallowness of the attractive well, it is to be expected that only the short-time dynamics of the stars will be determined by the clusters and long- or intermediate-time arrest within the clusters will not be present.[23] In this way, to obtain additional information about the cluster behavior, in the next section we explore the dynamical features of the system.

4 Dynamical characteristics of the clusters

In this section we turn our attention to the dynamical properties of the star/chain mixtures. A first step to gain some insight into the former ones is provided by the mean-square displacement (MSD) $\langle \Delta r_\alpha^2(t) \rangle$ (α = s, c), from which the self-diffusion coefficient D_α of each species can be calculated by means of the relation $D_\alpha = \lim_{t\to\infty} \langle \Delta r_\alpha^2(t) \rangle / 6t$. For all the simulated systems, the mean-square displacement has the characteristics of a simple ergodic fluid, *i.e*, a ballistic behavior at short times ($\langle \Delta r_\alpha^2(t) \rangle \sim t^2$) followed by a diffusive regime at larger ones ($\langle \Delta r_\alpha^2(t) \rangle \sim t$), as shown in the inset of Fig. 6 for $f = 18$ and $\rho_s\sigma_s^3 = 0.1$.

From those curves, we determine the chain density dependence of the star self-diffusion coefficient D_s, which is presented in Fig. 6 once it has been normalized to $D_s^{(0)}$, *i.e.*, its value in the absence of the chains. A sharp decrease of D_s is evident as chains are added, this decay being more pronounced for the lower star density, namely $\rho_s\sigma_s^3 = 0.05$. As can be seen, D_s tends to a plateau value, which can be rationalized by two compensating effects. In the first place, it is quite obvious that increasing the chain concentration will bring about a drop in D_s just because the stars are moving in a denser environment. However, as explained above, at a larger chain density the star–star potential $V_{ss}^{eff}(r)$ shows a shorter repulsive range, and therefore recovers some mobility by avoiding a further drop of D_s. Besides, as the number of star–star nearest neighbors increases, the stars move in an increasingly larger cluster environment.

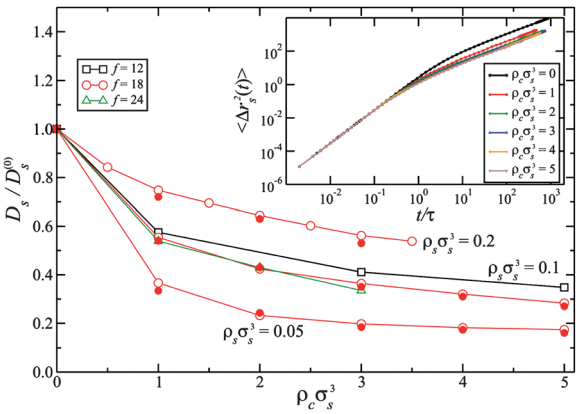

Fig. 6 Normalized self-diffusion coefficient of stars as a function of the chain density. Open symbols are results from simulations, while the filled ones come from theory for $f = 18$. Inset: Mean-square displacement for $f = 18$, $\rho_s\sigma_s^3 = 0.1$ and different chain densities.

Since no clear signature of clusters is found in the MSD, in order to gain additional insights into the dynamical behavior of the system, the relaxation of density fluctuations of wave-vector q was analyzed by means of the intermediate coherent and incoherent scattering functions. The coherent function is defined as

$$F_{\alpha\beta}(q,t) = \frac{\langle \rho_\alpha(q,t)\rho_\beta(-q,0)\rangle}{\langle \rho_\alpha(q,0)\rho_\beta(-q,0)\rangle} \tag{6}$$

and characterizes collective α-β correlations. In addition, we consider the incoherent function, which accounts for self-correlations, and is given by

$$F_\alpha^{(s)}(q,t) = \frac{1}{N_\alpha}\left\langle \sum_{j=1}^{N_\alpha} \exp\{ i\,\mathbf{q}\cdot[\mathbf{r}_{\alpha,j}(t) - \mathbf{r}_{\alpha,j}(0)]\}\right\rangle. \tag{7}$$

As expected from the MSD data, we found a monotonic decay of the self-correlation $F_\alpha^{(s)}(q,t)$ as Fig. 7(a) shows for the wave-vector $q\sigma_s = 1$, which is related to the location of the cluster peak (see Fig. 1), and $f = 18$. The decay time increases only slightly at higher chain densities, due to the previously mentioned antagonistic effect between density and reduction of the short-repulsion range of $V_{ss}^{eff}(r)$. On the other hand, Fig. 7(b) displays star–star coherent correlation function for the same density as before and two functionalities, *i.e.*, $f = 18$ and $f = 24$. In absence of chains, $F_{ss}(q,t)$ shows an oscillatory behavior corresponding to a propagating sound mode, the amplitude and frequency of which, increase with the star density. Since in our simulations Newtonian dynamics was

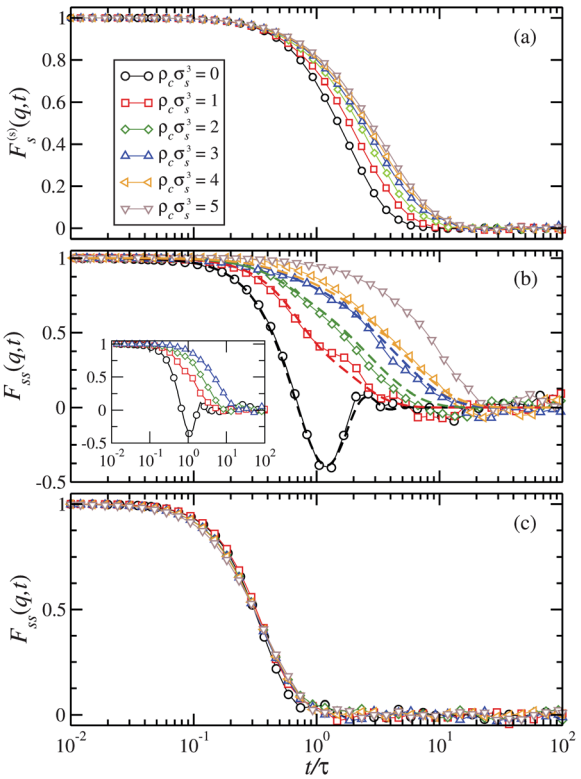

Fig. 7 (a) Incoherent and (b) coherent star–star correlation function for $f = 18$ at $q\sigma_s = 1.0$. Symbols and dashed lines correspond to simulation and theory, respectively. Inset: Coherent correlation function for $f = 24$. (c) Coherent star–star correlation function for $f = 18$ at $q\sigma_s = 4.2$. In all cases $\rho_s\sigma_s^3 = 0.1$.

employed and an explicit solvent was not included, the attenuation of this mode is very weak. The real dynamics of the pure star suspensions would be represented more suitably by employing, for example, Brownian dynamics, for which these oscillations are expected to be washed out. In fact, once chains are included in the system, that mode is strongly damped even for the lowest (finite) chain density considered. Although the coherent scattering function $F_{ss}(q,t)$ completely relaxes, pointing out the star dynamics are ergodic at both the particle ($q\sigma_s \sim 4$, Fig. 7(c)) and the cluster scales ($q\sigma_s \sim 1$, Fig. 7(b)), at the latter scale the system features a significantly slower structural relaxation as the chain density is increased. This suggests the presence of a transient cooperative dynamics within the cluster, lasting up to $\sim 10\tau$. The slowing-down persists, even if the unit of time τ is rescaled for each chain density according to $\tau \to \tilde{\tau} = (D_s^{(0)}/D_s)\tau$, which corrects to some extent the direct effect on the stars due to the presence of an increasing denser (chain) background, supporting the statement above.

As mentioned previously, the picture for the cluster formation in the system at hand is reminiscent of the one found in colloid–polymer mixtures.[3,24,26] However, the two systems bear a very important difference. Since a pure star suspension in the regime of considered functionalities remains fluid at any density,[35,36] then star/chain mixtures will be driven to a complete phase separation at high enough chain density, in contrast to the colloid/polymer mixtures for which gel-like states can be reached *via* an arrested phase separation.

In order to provide a theoretical description of the phenomenology of the system, we compare simulation results with those from a theoretical treatment of diffusion based on mode-coupling-theory (MCT), which provides a clearer physical picture of the dependence of the self-diffusion constant on the microscopic parameters of the system. In this way, in computing the star self-diffusion coefficient D_s in the star–linear polymer mixture, we follow earlier work in binary mixtures.[37,38] The star self-diffusion constant D_s is given by the total time integral of the (normalized) star velocity time correlation function (TCF)

$$D_s = \frac{k_B T}{m_s}\int_0^\infty dt\; C_s(t) \tag{8}$$

with

$$C_\alpha(t) = \frac{\langle \mathbf{v}_\alpha(t)\cdot\mathbf{v}_\alpha(0)\rangle}{\langle \mathbf{v}_\alpha(0)\cdot\mathbf{v}_\alpha(0)\rangle}. \tag{9}$$

The Laplace transform of the TCF, $\tilde{C}_s(z)$, can be written in the form of a continued fraction as follows:[22,39]

$$\tilde{C}_s(z) = \cfrac{1}{z + \cfrac{K_1(0)}{z + \tilde{K}_2(z)}}, \tag{10}$$

where $K_i(t)$ and $\tilde{K}_i(z)$ are, respectively, the i-th order memory function of $C_s(t)$ and the corresponding Laplace transform. The microscopic expression for $K_1(0)$ is well-known:[22,39]

$$K_1(0) = \frac{1}{3m_s}\int d\mathbf{r}\left[\rho_s\, g_{ss}(r)\,\nabla^2 V_{ss}(r) + \rho_c\, g_{sc}(r)\nabla^2 V_{sc}(r)\right], \tag{11}$$

corresponding to the (squared) Einstein frequency for the stars. With the above, the star self-diffusion coefficient is given by[22,39]

$$D_s = \frac{k_B T}{m_s}\frac{\tilde{K}_2(0)}{K_1(0)}. \tag{12}$$

It follows from the above that the star self-diffusion coefficient can be obtained from the second-order memory function $K_2(t)$. In the present work, we compute $K_2(t)$ within the MCT formalism. The corresponding expression, involving a sum of star–star and star–chain memory functions, is given by eqn (12) of Ref. 37; it is rather lengthy and will not be reproduced here. Suffice it to say that it requires as input the star incoherent correlation function $F_s^{(s)}(q,t)$, as well as the star–star and chain–chain coherent correlation functions $F_{ss}(q,t)$ and $F_{cc}(q,t)$, respectively. For the former, we adopt the well-known Gaussian approximation[39]

$$F_s^{(s)}(q,t) = \exp\left[-\frac{k_B T}{m_s}q^2\int_0^t ds(t-s)C_s(s)\right], \tag{13}$$

while coherent correlation functions are obtained from continued fraction representations of their respective Laplace transforms. For example, the Laplace transform of the star–star coherent correlation function (truncated at the second order) is written as:[22,39]

$$\tilde{F}_{ss}(q,z) = \cfrac{1}{z + \cfrac{\delta_1(q)}{z + \cfrac{\delta_2(q)}{z + \tau_0^{-1}(q)}}}, \tag{14}$$

where $\delta_i(q)$ is the initial time value of the i-th order memory function of $F_{ss}(q,t)$. For the parameter $\tau_0^{-1}(q)$ we use the expression $\tau_0^{-1}(q) = 2\sqrt{\delta_2(q)/\pi}$ given by Lovesey.[40] The quantities $\delta_1(q)$ and $\delta_2(q)$ can be easily calculated from the first three short-time expansion coefficients of $F_{ss}(q,t)$; the microscopic expressions for the latter are well-known and will not be reproduced here.[41] The calculation of the chain–chain coherent correlation function is based on the same procedure.

In order to test the accuracy of the theory outlined above, we compare theoretical predictions with results of MD simulations. To this end, theoretical results for $F_{ss}(q,t)$ obtained from eqn (14) are shown together with the MD data in Fig. 7(b) for several values of chain concentration, $f = 18$, $\rho_s\sigma_s^3 = 0.1$, and $q\sigma_s = 1.0$. The agreement between theory and simulation is seen to be good at all chain concentrations except for the highest one, where theory somewhat overestimates the long-time tail of the coherent correlation function. Since the approximation considered for $F_{ss}(q,t)$ is based on its short-time expansion and, as such, it cannot *a priori* be expected to be accurate at long times, it is remarkable that it works well at long times for a wide range of chain densities. A more appropriate treatment of long-time behavior of the coherent correlation functions would involve solving self-consistently a full coupled system of MCT equations both for chains and stars,[42] which is numerically demanding and beyond the scope of this work.

Having confirmed the accuracy of our theoretical approach in calculating the dynamic quantities needed as input for our MCT treatment of the diffusion coefficient, we next compute the star self-diffusion coefficient as outlined above. Our results for D_s (normalized to its value in the absence of chains) are shown in Fig. 6 together with the simulation data; the agreement between theory and simulation is satisfactory. Since the long time behavior of $K_2(t)$ is dominated by the transverse current correlation functions $C_t(q,t)$ and not by $F_{ss}(q,t)$ (the first term in eqn (12) in Ref. 37), then the MCT scheme works better for $C_t(q,t)$ (also based on its short-time expansion) than for $F_{ss}(q,t)$.

5 Conclusions

In this work, we have studied the formation of clusters in mixtures of star- and linear polymers. By using a coarse-grained description of the interactions between the components, we performed full, two-component Molecular Dynamics simulations to investigate both structural and dynamical behavior of the mixtures. The accuracy of such a coarse-grained description of the star/chain mixture has been recently tested against experiments in a wide range of concentrated mixtures, finding quantitative agreement between experiments and theory for the influence of the added chains on the star–star structure and on their phase behavior.[20]

For low and intermediate volume fractions ($\rho_s/\rho_s^* \lesssim 0.35$) and low-functionality ($f \lesssim 24$) star polymer suspensions, the addition of polymer chains yield to the formation of polydispersed and transient aggregates, *i.e.*, clusters, as evidenced by the rise up of a pre-peak at low wave-number in the static structure factor $S_{ss}(q)$ and the slight slowing-down of the collective correlation function $F_{ss}(q,t)$ at the same wavelength. This cluster formation is driven by entropy leading to an incipient phase separation so that, upon a further increase of the chain density, the small star aggregates begin to form a transient network which span the whole simulation box. We found that stars stick reversibly upon approach to form structures, where the size dependence on the number of connected particles is similar to that of the structures resulting from reaction-limited cluster aggregation (RLCA), as demonstrated by the distribution of cluster sizes.

The aforementioned scenario can be rationalized by employing the framework of depletion interaction, as in the case of hard colloids/polymer mixtures. This allows one to trace the properties of the cluster formation to two main features of the chain-modified star–star interaction $V_{ss}^{eff}(r)$, which permits an effective one-component description of the mixture. In the first place, the unusual characteristic of the system, pertaining to the range of the chain-induced depletion attraction, which in strong contrast to both binary hard-spheres mixtures and colloid/polymer mixtures, does not depend on the size of the depletant particles; and secondly, the shrinkage of the star polymers as consequence of the osmotic force exerted by the chain polymers. Since there are other systems sharing the star-like behavior, *i.e.* micelles, dendrimers, grafted nanoparticles, and in general core–shell particles, we expect that the described picture would be similar in other soft matter systems.

In that sense, the fact that a second level coarse-graining of the mixture can be carried out by introducing an adequate mapping to the effective one-component description $V_{ss}^{eff}(r)$, leading to the same structural information could be of great interest. Since that mapping would make a complete self-consistent MCT treatment (*i.e.*, without to resort to short-time expansions) of the dynamic functions much more feasible, it would be providing further details concerning the cluster dynamics and its consistency with the "static" interpretation.

Acknowledgements

This work has been supported by the project ITN-234810-COMPLOIDS (Marie Curie Training Network, EU), the Network of Excellence SoftComp, and the Wolfgang Pauli Institute (WPI), Vienna. M.C. thanks UAN-ICETEX-Colciencias (Colombia) and DAAD (Germany) for a PhD fellowship through the ALECOL Program.

References

1 W. C. K. Poon, *J. Phys.: Condens. Matter*, 2002, **14**, R859.
2 P. J. Lu, J. C. Conrad, H. M. Wyss, A. B. Schofield and D. A. Weitz, *Phys. Rev. Lett.*, 2006, **96**, 028306.
3 J. C. Conrad, H. M. Wyss, V. Trappe, S. Manley, K. Miyazaki, L. J. Kaufmann, A. B. Schofield, D. R. Reichmann and D. A. Weitz, *J. Rheol.*, 2010, **54**, 421.
4 D. Vlassopoulos and G. Fytas, *Adv. Polym. Sci.*, 2010, **236**, 1.
5 C. Mayer, F. Sciortino, C. N. Likos, P. Tartaglia, H. Löwen and E. Zaccarelli, *Macromolecules*, 2009, **42**, 423.
6 E. Stiakakis, D. Vlassopoulos, C. N. Likos, J. Roovers and G. Meier, *Phys. Rev. Lett.*, 2002, **89**, 208302.
7 E. Stiakakis, G. Petekedis, D. Vlassopoulos, C. N. Likos, H. Iatrou, N. Hadjichristidis and J. Roovers, *Europhys. Lett.*, 2005, **72**, 664.
8 C. N. Likos, C. Mayer, E. Stiakakis and G. Petekedis, *J. Phys.: Condens. Matter*, 2005, **17**, S3363.
9 F. Sciortino, S. Mossa, E. Zaccarelli and P. Tartaglia, *Phys. Rev. Lett.*, 2004, **93**, 055701.
10 F. Cardinaux, A. Stradner, P. Schurtenberger, F. Sciortino and E. Zaccarelli, *Europhys. Lett.*, 2007, **77**, 48004.
11 C. N. Likos, A. Lang, M. Watzlawek and H. Löwen, *Phys. Rev. E: Stat. Phys., Plasmas, Fluids, Relat. Interdiscip. Top.*, 2001, **63**, 031206.

12 B. M. Mladek, D. Gottwald, G. Kahl, M. Neumann and C. N. Likos, *Phys. Rev. Lett.*, 2006, **96**, 045701.
13 C. N. Likos, *Phys. Rep.*, 2001, **348**, 267.
14 C. Mayer and C. N. Likos, *Macromolecules*, 2007, **40**, 1196.
15 C. N. Likos, H. Löwen, M. Watzlawek, B. Abbas, O. Jucknischke, J. Allgaier and D. Richter, *Phys. Rev. Lett.*, 1998, **80**, 4450–4453.
16 A. Jusufi, J. Dzubiella, C. N. Likos, C. von Ferber and H. Löwen, *J. Phys.: Condens. Matter*, 2001, **13**, 6177.
17 R. L. C. Vink, A. Jusufi, J. Dzubiella and C. N. Likos, *Phys. Rev. E: Stat., Nonlinear, Soft Matter Phys.*, 2005, **72**, 030401.
18 M. Daoud and J. P. Cotton, *J. Phys.*, 1982, **43**, 531.
19 M. Laurati, J. Stellbrink, R. Lund, L. Willner, D. Richter and E. Zaccarelli, *Phys. Rev. Lett.*, 2005, **94**, 195504.
20 B. Lonetti, M. Camargo, J. Stellbrink, C. N. Likos, E. Zaccarelli, L. Willner, P. Lindner and D. Richter, *Phys. Rev. Lett.*, 2011, **106**, 228301.
21 D. Frenkel and B. Smit, *Understanding molecular simulations*, Academic Press, London, 2002.
22 J. P. Hansen and I. R. McDonald, *Theory of simple liquids*, Academic Press, London, 2006.
23 Y. Liu, L. Porcar, J. Chen, W. R. Chen, P. Falus, A. Faraone, E. Fratini, K. Hong and P. Baglioni, *J. Phys. Chem. B*, 2011, **115**, 7238.
24 P. J. Lu, E. Zaccarelli, F. Ciulla, A. B. Schofield, F. Sciortino and D. A. Weitz, *Nature*, 2008, **453**, 499.
25 M. Y. Lin, H. M. Lindsay, D. A. Weitz, R. C. Ball, R. Klein and P. Meakin, *Phys. Rev. A*, 1990, **41**, 134907.
26 M. Laurati, G. Petekidis, N. Koumakis, F. Cardinaux, A. B. Schofield, J. M. Brader, M. Fuchs and S. U. Egelhaaf, *J. Chem. Phys.*, 2009, **130**, 134907.
27 M. Camargo and C. N. Likos, *J. Chem. Phys.*, 2009, **130**, 204904.
28 M. Camargo and C. N. Likos, *Phys. Rev. Lett.*, 2010, **104**, 078301.
29 A. Wilk, S. Huissmann, E. Stiakakis, J. Kohlbrecher, D. Vlassopoulos, C. N. Likos, G. Meier, J. K. G. Dhont, G. Petekidis and R. Vavrin, *Eur. Phys. J. E*, 2010, **32**, 127.
30 D. Truzzolillo, D. Vlassopoulos and M. Gauthier, *Macromolecules*, 2011, **44**, 5043.
31 Y. Liu, W. R. Chen and S. H. Chen, *J. Chem. Phys.*, 2005, **122**, 044507.
32 A. Fierro, T. Abete, A. Coniglio and A. de Candia, *J. Phys. Chem. B*, 2011, **115**, 7281.
33 A. Stradner, H. Sedgwick, F. Cardinaux, W. C. K. Poon, S. U. Egelhaaf and P. Schurtenberger, *Nature*, 2004, **432**, 492.
34 F. Cardinaux, E. Zaccarelli, A. Stradner, S. Bucciarelli, B. Farago, S. U. Egelhaaf, F. Sciortino and P. Schurtenberger, *J. Phys. Chem. B*, 2011, **115**, 7227.
35 M. Watzlawek, C. N. Likos and H. Löwen, *Phys. Rev. Lett.*, 1999, **82**, 5289–5292.
36 G. Foffi, F. Sciortino, P. Tartaglia, E. Zaccarelli, F. Lo Verso, L. Reatto, K. A. Dawson and C. N. Likos, *Phys. Rev. Lett.*, 2003, **90**, 238301.
37 S. A. Egorov, *J. Chem. Phys.*, 2003, **119**, 4798.
38 L. A. Shall and S. A. Egorov, *J. Chem. Phys.*, 2010, **132**, 184504.
39 U. Balucani and M. Zoppi, *Dynamics of the liquid state*, Clarendon, Oxford, 1994.
40 S. W. Lovesey, *J. Phys. C: Solid State Phys.*, 1971, **4**, 3057.
41 D. L. Price and J. R. D. Copley, *Phys. Rev. A: At., Mol., Opt. Phys.*, 1975, **11**, 2124.
42 E. Flenner and G. Szamel, *Phys. Rev. E: Stat., Nonlinear, Soft Matter Phys.*, 2005, **72**, 031508.

